Journal of Complex Flow, Vol. 4 No. 2 (2022) p. 6-12

Journal of Complex Flow

Journal homepage: www.fazpublishing.com/jcf

e-ISSN: 2672-7374



Airflow Behavior of Quadcopter Fertilizer Drone for Pineapple Plantation by Using CFD

Khiew Vun Fung¹, Omar Mohd Faizan Marwah^{1,*} Siti Juita Mastura Mohd Saleh², Mohammad Zulafif Rahim²

- ¹ Faculty of Mechanical and Manufacturing Engineering, Universiti Tun Hussein Onn Malaysia, Batu Pahat, 86400, MALAYSIA
- ² Avitex Solution (M) Sdn. Bhd, Universiti Tun Hussein Onn Malaysia (UTHM), Batu Pahat, 86400, MALAYSIA

Received 24 July 2022; Accepted 14 August 2022; Available online 1 Sept. 2022

Abstract: UAV can efficiently complete fertilization operations, regardless of the geographic factor, without the need for dedicated landing sites. The effective coverage and velocity of downwash are directly related to the assemblage of the spraying system and the spraying effect. However, the unclearness of the airflow field leads to a severe droplet drift problem. In this study, the simulation on airflow behavior by using the CFD method is done for optimization of sprayer efficiency by analyzed the current designation of sprayer system and proposed an appropriate range for nozzle working position. The transient analysis simulation is done with the SST k-w turbulence model using Ansys Fluent Software to observe and analyze airflow vector, velocity contour, and downwash velocity. Simulation results show inward curve flow at an area 1.5 meters below the rotor and high-velocity regions spotted at 1.0 meters below the rotor at the central region and 0.6 meters vertically below the rotor. The working height is suggested to be 1.06 meters below the rotor with nozzle spacing of 0.9 meters for each side and 0.7 meters from the center. The working position is at the central area between sets of rotors.

Keywords: CFD transient simulation, Ansys Fluent, Agriculture Crop Dusting Quadcopter, K-w SST turbulence model

1. Introduction

Unmanned Aerial Vehicles (UAVs), commonly mentioned as drones, go through massive development in various fields rapidly, starting from military use. UAVs such as quadcopters is then used for dusting crops, plant monitoring, spraying etc., to replace the use of slow-paced human workforces starting 1900s. Malaysia's farmers still using the traditional method for fertilizing tasks such as manually, knapsack sprayer and tractor-mounted highpressure sprayer [1]. According to Sem (2020), the drone can apply plantation aiding liquid more economically than traditional ways. Pesticides can save up to 20% [2]. Studies on agriculture initially focus on crop production and protection material (fertilizer and pesticides) efficiency and their impact on soil or the surrounding environment [3]. An extensive study on agriculture drones focused on sprayer efficiency proved that the selection of sprayer design parameters such as sprayer nozzle, sprayer location, sprayer boom height, etc., are the critical roles of cropdusting efficiency [4]. Since aerial spraying is a method of transporting liquid onto the crops through a combined wind field, airflow became dominant in controlling droplet deposition.

The combination of airflow generated by propeller rotation with atmospheric wind and downwash caused by ground effect and flight altitude will result the combined wind field. The airflow field produced by UAV plays a key role in droplet transportation during crop-dusting activity [5]. Hence it is an important issue to get a perfect location for a sprayer.

Reviewing previous studies shows that there are mainly two UAV airflow field analysis methods: experimental or numerical. The typical approach of experimental is wind tunnel experiment or analyzes data collected through water-sensitive paper, mylar, or monofilament lines. The numerical method is studying the programmed software such as ANSYS or Solidworks simulated model associated with CFD theory. Both ways give the same trend of result, but numerical would be more appropriate for complicated situations because some situations are hard to demonstrate through experiments. Hector Guillermo et al. [6] used CFD to perform transient analysis on aerodynamic behavior's physical variables, verifying that numerically obtained aerodynamic behavior analysis is practical to support future research.

^{*}Corresponding Author

The difference of value in experimental and numerical results is between 0.6 to 0.7, which assured the reliability of simulation data in UAVs' aerodynamic behavior study. [7]. Suggestions are made through observing airflow behavior on design and operating specification such as sprayer nozzle, flight speed, hovering height are also given in several studies [5], [8-11]. Observing the airflow field pattern also provides information on several parameters that strengthen the droplet deposition, as proven by Xue et al. [12]. The study concluded that downwash airflow generated by the aerial spraying device's rotor could strengthen the agrochemical penetration droplet on the under/ lower layer of crops compared to the traditional spraying method.

Simultaneously, the fertilizing task of PINEXRI-20 needs to get droplets deposited on the root area to maximize its efficacy. The main purpose of this research is to find the optimal range for the sprayer system working location. To archive this, the analysis of the airflow velocity and pattern was done with the help of CFD simulations. Once the results are delivered, the most expected results were highlighted through the velocities data and simulated contours. The paper's organization is as follows: In Section 2, the definition of the geometric model and simulations method for three different hovering operating parameters was described. Next, the simulated results are presented, and simulated velocities data and contours were discussed in Section 3. Finally, conclusions are drawn based on the above study in Section 4.

2. Materials and Methods

In this research, the quad-rotor pineapple plantation fertilizing drone PINEXRI-20 was selected as a model for the numerical analysis to narrow down unnecessary parts. To save on computer resources, the physical model of the drone was rationally simplified and left only the body frame, rotors, propeller, and sprayer nozzle. An external power supply powered the drone, and a wireless remote controller regulated the rotor rotational speed.

2.1 Model establishment and computational domain

The rotors are important parts of the drone that generate the airflow field and the necessary lift for the drone on hovering. In this study, the model is established with four 29 inches propeller blades with a 9.5 pitch. Solidworks 2019 is used to construct the 3D model with rotors of clockwise rotation and anticlockwise rotation, respectively, as shown in Figure 1. The model assembly is analyzed with CFD using Ansys Fluent Software, to achieve adequate simulation results, domains are constructed using Design Modeler to cover the body to avoids the construction of high detail mesh.

The global square stationary domain shows in Figure 3 and 4 with width 4 meters and 2 meters height defined for the inlet and outlet airflow while the four subdivided rotational domains with 0.8 meters diameter and 0.2 meters height represent the rotors.



Fig. 1 - Isometric View of PINEXRI-20 3D Model

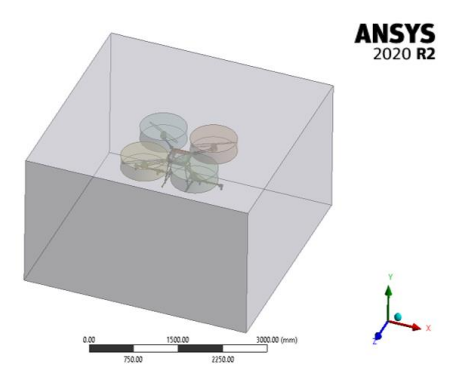


Fig. 2 - Stationary Domain

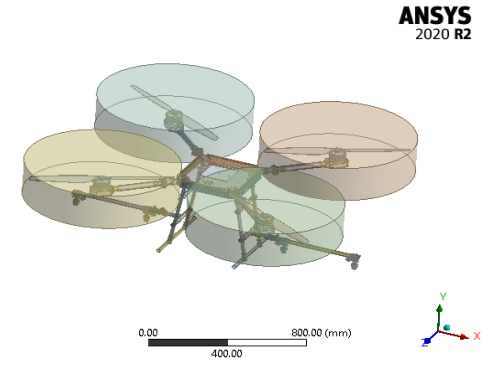


Fig. 3 – Rotating Domain

Besides that, only the rotor and domains of the drone are considered in the computational model because the rotors are far from the fuselage which other parts have only minimal influence on airflow [8], [13] while other parts are suppressed, as in Figure 4.

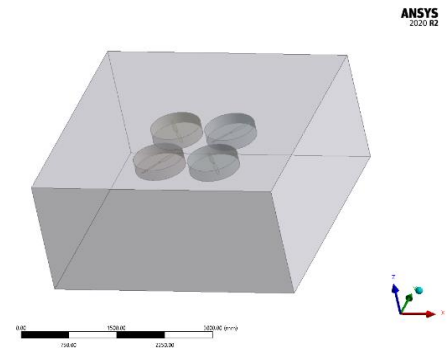


Fig. 4 – Computational Geometry

2.2 Mesh Generation

Meshing is the process of discretizing the computational domain into grids with elements and nodes. The grid quality will affect the rate of convergence, performance of numerical analysis and computational time. Due to the irregular surface of rotor propeller and it is the most crucial part in the numerical simulation, an unstructured triangular grid was adopted. The mesh on the tip and contact region increased, and the resultant meshed are shown in Figure 5 and Figure 6; the total number of nodes was 148886, and the total number of elements was 711077. Grid independence study was performed on five different grids by varying sizes of the element to find the most suitable mesh for this study and ensure simulation stability.

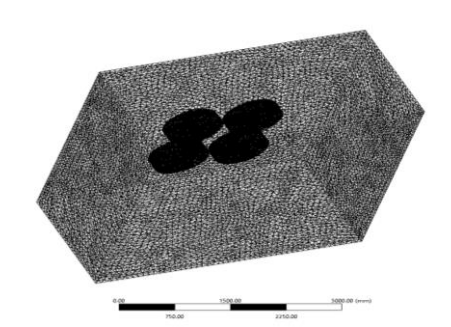


Fig. 5 - Overview of Computational Domain Mesh

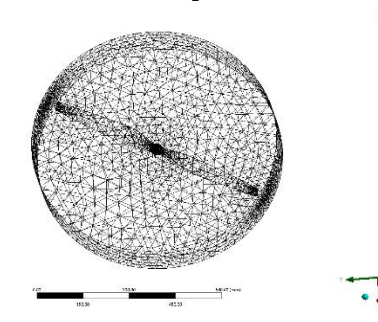


Fig. 6 – Mesh of Rotational Domain

2.3 Boundary Conditions and Calculation Methods

CFD simulations were conducted in the hovering operating condition as summarized in Table 1. The working medium was set as air and other parameters remain default to simulate airflow condition by not considering other environmental effects such as crosswind. Since the simulation was for the quadrotor fertilizing UAV in hovering state, throttle percentages are selected as 50%,60% and 75% based on the standard design specification of UAV as higher percentages are used for accelerating during takeoff. On the inlet boundary, velocities are specified respected to thrust and the pressure outlet boundary with respect to atmospheric pressure was used. The data between the static domain and four rotation domains are exchanged through the interface boundary. The direction of gravitational acceleration is along the negative direction of the z-axis. Mesh motion adapted at four-rotor to illustrate the clockwise and anticlockwise propeller rotation as illustrated in Figure 7.

The rotation axis origin and direction were set according to the actual situation. Furthermore, the SST k-w turbulence model was selected, which is suitable for complex shear stress flow [8], [11], [14], [15] because the downwash flow is caused by the rotor rotating at high speed to calculate 180 timesteps for each case.

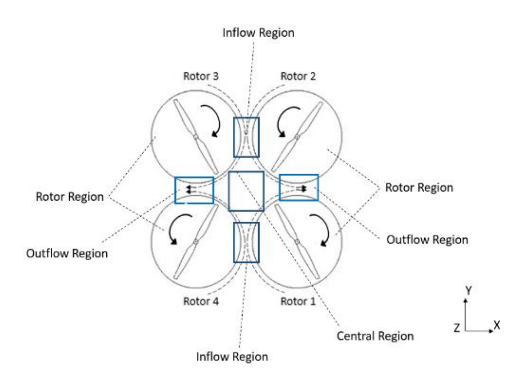


Fig. 7 – Schematic diagram of Computational Domain

Table 1 - Setting Details for different RPM

Case	Throttle (%)	Thrust (g)	RPM	Timestep size (s)	Inlet Velocity (m/s)
1	50	3700	2195	3.7965x10-4	11.7910
2	60	5280	2599	3.2064x10-4	14.0854
3	75	7710	3123	2.6684x10-4	17.0208

3. Results and Discussion

3.1 Analysis of Flow Vector

The results show a circular flow region at region labelled 1 in Figure 8. The occurrence of circular flow may result the backflow of fertilizer and cause waste in fertilizer due to ineffective spraying operation. The flow line in the region labelled 2 shows a high tendency to form an upward circular flow and cause a drift phenomenon. The flow line at 0.5 meters away from the quadcopter remains straight, indicating the propeller's rotating effect not affecting the airflow that is 0.5 meters away from the quadcopter, also known as the buffer zone. When the altitude decreases and close to the ground at -1.5 meters vertical distance, the flow starts to curve inward. When the airflow reaches the ground, this phenomenon can be explained by z-direction velocity transverse to x-direction and y-direction velocity and causing the airflow detent around the ground, also known as ground effect.

This inward curve can help strengthen fertilizer penetration on pineapples' roots or the lower side of the plant canopy. According to the flow pattern, we can conclude that the nozzle should be placed at least 0.5 meters below the rotor and avoid the circular region and drifting regions marked in Figure 8.

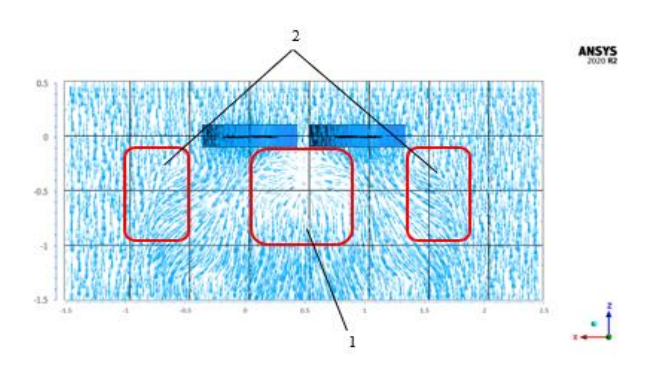
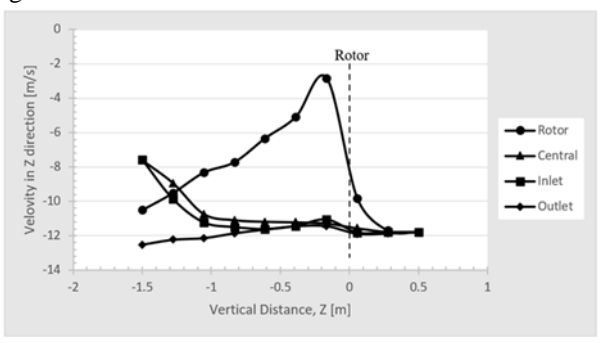


Fig. 8 – Flow Vector of Airflow Generated by Rotor Motion.
1. Circular Flow Region 2. Drifting Region

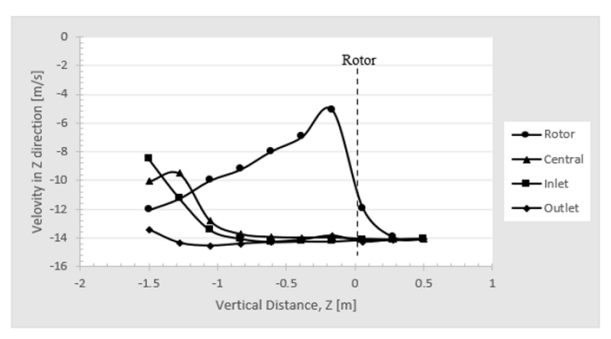
3.2 Downwash flow velocity in the z-direction at different regions

To demonstrate the relationship between flight speed and the quadcopter downwash flow velocity in the zdirection at the different regions (inflow region, outflow region, rotor region and central region) is measured and studied as in Figure 7. Velocity in the z-direction is observed and discussed in this section because z-direction velocity affects downwash and will restrain the drift and strengthen the deposition rate of fertilizer on pineapple plants [8], [13]. The results of downwash velocity are presented in Figure 9 with negative y-axis velocity, which indicated the downward velocity flow fields. As observed from the graphical results, the velocity above the gives the highest value at the same time for all four regions, which is 2 meters above the ground and 0.5 meters above the rotor. This can be explained by the suction effect that occurred above the rotor. The high rotating speed of the quadcopter results in identical downward velocity toward the rotor direction to create suction force.

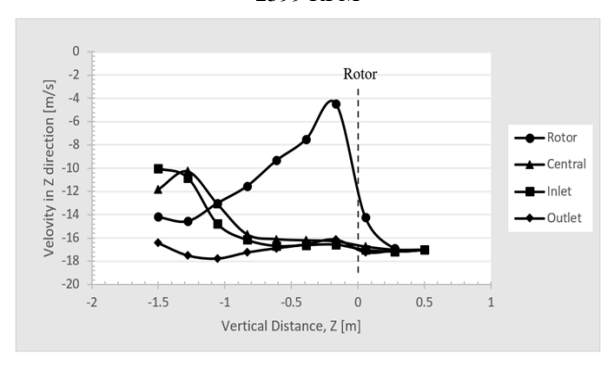
On the other hand, the rotor regions have the most significant fluctuation correspond to other regions. This is proof that this region having the highest probability inhibit drift phenomena. In the zone starting 1.33 meters from the ground, the *z*-direction velocity increases rapidly and reaches its maximum, 10.51 ms⁻¹ when it comes to the ground. This is probably because the downwash airflow spread to the surrounding can create a rebound of flow when it contacts the ground. Hence, through comparison between three sets of data, the *z*-direction velocity is arranged as follows: inlet region > central region > outlet region.



2195 RPM







3123 RPM

Fig. 9 –Downwash velocity distribution of vertical distance in different regions for various rotational speeds

3.3 Analysis of velocity contour

In this section, the velocity contour plot shown is area along the central region and outflow region as in Figure 10 and area under the rotor and inflow region in Figure 11. From the contour plot, the relationship between rotor rpm and airflow velocity is directly proportional. This proven by the maximum velocity data of both conditions represent in Table 2 and 3. Increment in rotational speed of rotor able to increase the air velocity and strengthen the spraying force.

From the contour plot, the red zone shown in velocity contour can be considered as a reference for plant position during spraying activities designation to increase the rate of spray efficiency. The high velocity can improve the spraying strength of fertilizer and increase the deposit chance of fertilizers on the plant's root. In Figure 11, the rotor is located at -1 meters and 0 meter of the *x*-axis, origin of the y axis in the contour plot. Downwash flow is shown in the orange plot below the rotor. This phenomenon can be explained that the airflow velocity under the rotor contributes to the central region for hovering. Overlapping of airflow due to the rotor operating principle in reverse rotation forms a hedging phenomenon and creates constant thrust for hovering.

By comparing the velocity data at the central region and outflow region with the data at the region under the rotor there is a clear difference in high-velocity area distribution. The central region and outflow region have a larger coverage area of the high-speed region and a higher maximum velocity value. Hence, sprayer system would be more suitable located at the central region and outflow region.

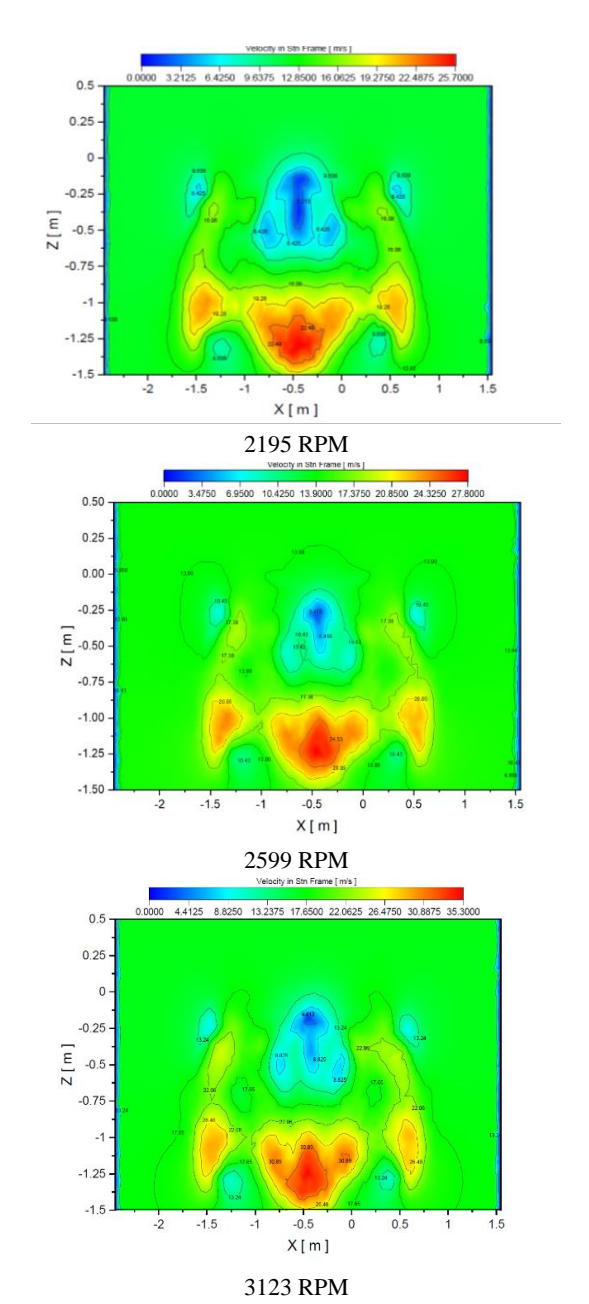


Fig. 10 –Velocity contour at central region and outflow region for various rotational

Table 2 - Data at central region and outflow region

Throttle Percentage (%)	RPM	Max Velocity (m/s)
50	2195	25.70
60	2599	27.80
75	3123	35.30

Table 3 - Data at region under the rotor

	_	
Throttle Percentage (%)	RPM	Max Velocity (m/s)
50	2195	19.40
60	2599	22.70
75	3123	28.40

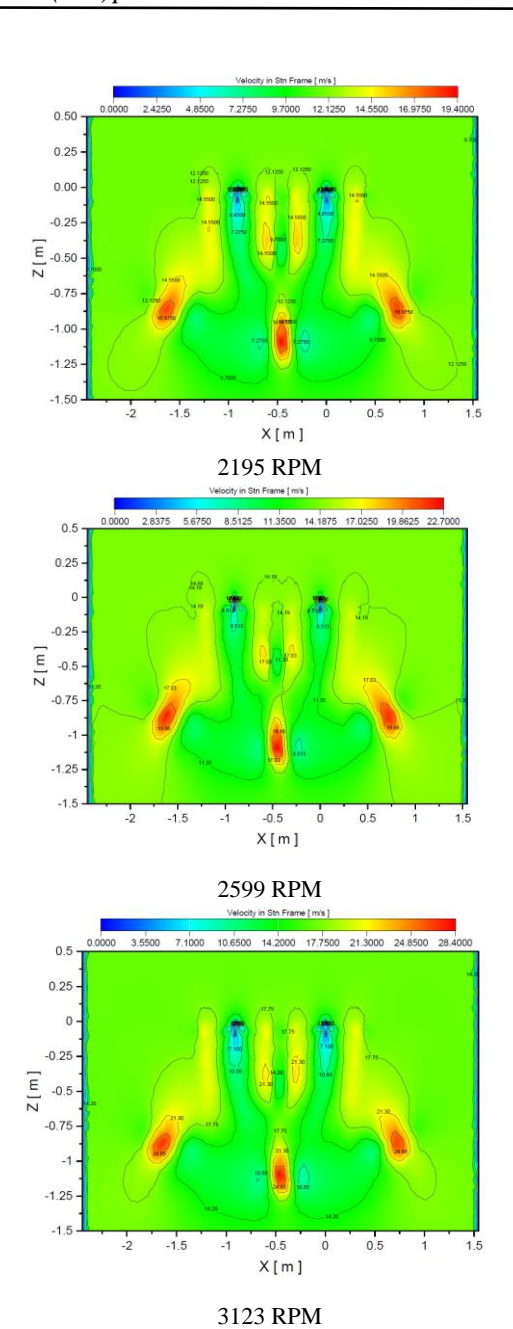


Fig. 11 –Velocity contour at region under the rotor for various rotational speeds

3.4 Analysis of current PINEXRI-20 designation

The current design of PINEXRI-20 sets the boom position at 0.4 meters under the rotor and has a nozzle at the central region with 0.5 meters nozzle spacing. In this study, horizontal airflow velocity is analyzed to identify the suitable location for the nozzle position and vertical airflow velocity to determine the appropriate height for the boom position. The plotted graph line of three different rotational speeds for horizontal airflow velocity showing the same trendline with an increasing velocity trend as in Figure 12. From the plotted results, velocity show steady in trend at an area 1.5 meters away from the center for both positive and negative plot.

This can be explained by the airflow 1.5 meters away from the center no longer affected by the high-speed rotation motion of the rotor propeller. It can be observed from the graph that the maximum velocity occurs at -0.62m, -1.51m and 0.71m and 1.6m of *x*-axis. Since the area with higher velocity is ideal for installing a spray nozzle, the spray nozzle should be placed at the maximum velocity locations.

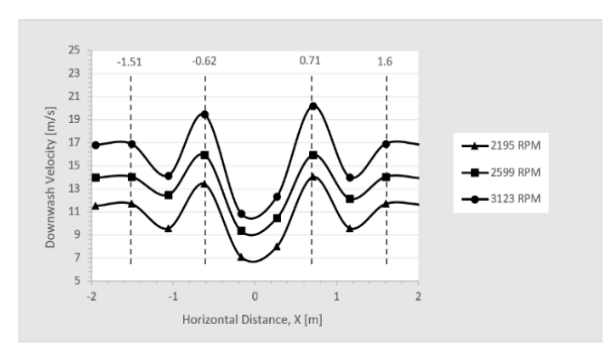
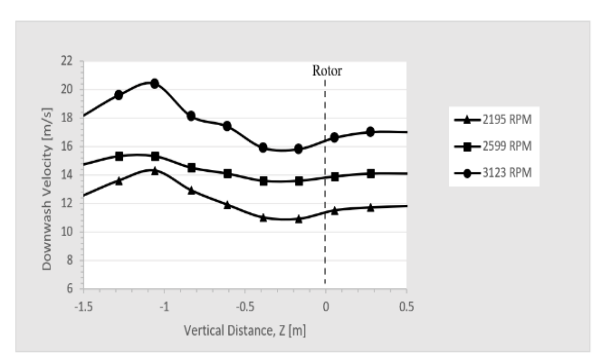


Fig. 12 –Downwash velocity distribution of airflow along horizontal distance x for various rotational speeds

The vertical airflow velocity was investigated at nozzle 1 and nozzle 2 locations with nozzle spacing 0.5 meters shown in Figure 13. For the nozzle 1 location, the velocity increases gradually, starting 0.5 meters below the rotor and archive the highest velocity at around 1.06 meters below the rotor. In contrast, nozzle 2 location shows unstable fluctuation in vertical airflow velocity. Despite that, maximum velocity also occurs at around 1.06 meters below the rotor.



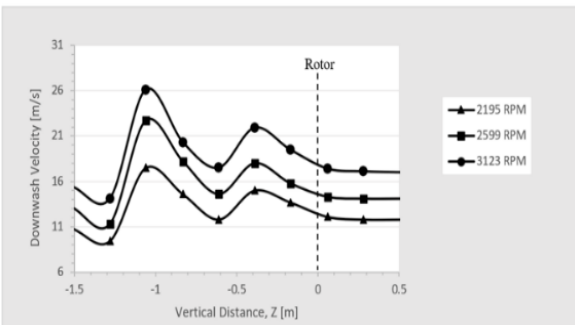


Fig. 13 –Downwash velocity distribution of airflow along vertical distance x for various rotational speeds (Nozzle 1 – above, Nozzle 2 – below)

4. Conclusion

The downwash velocity flow fields at different rotor rotational speeds were studied through CFD simulation to improve the spraying system efficiency through determination of optimal location for sprayer nozzle. Hence, the objective of study had achieved. The flow vector was presented, showing an inward curve flow at an area 1.5 meters below the rotor, increasing the deposition rate of fertilizer on crops' root area. The airflow vector also shows the downwash airflow pattern and identified the area with a high tendency to drift.

The study presented the velocity contour at the central region between two rotors and the region under the rotor, which showing the high-velocity regions are located at 1.0 meters below the rotor at the central region and 0.6 meters below the rotor for the region under the rotor, which provides a reference to determine the aerial spraying strength. By comparison, the maximum velocity values and the red zone coverage of central outflow regions are higher than the region under the rotor. This indicates that it is more appropriate to install a nozzle in central outflow region as a working position.

An optimal solution for a quadcopter with P80 KV100 motor's ideal spraying nozzle location is determined by analyzing the results of velocity data in different regions and positions by observing the data. The working height is more appropriate to be 1.06 meters below the rotor with nozzle spacing 0.9 meters for each side and 0.7 meters from the center. The working position is at the central area between sets of rotors.

Acknowledgment

The authors would like to thank the Faculty of Mechanical and Manufacturing Engineering, Universiti Tun Hussein Onn Malaysia, and Avitex Solution (M) Sdn. Bhd for data support and giving the opportunity to conduct this study.

References

- [1] A. M. Nazri and D. E. Pebrian, "Analysis of energy consumption in pineapple cultivation in Malaysia: A case study," *Pertanika J. Sci. Technol.*, vol. 25, no. 1, (2017): pp. 17–28.
- [2] P. Sem, "Crop-dusting drones making work safer and easier for farmers | Science| In-depth reporting on science and technology | DW | 21.02.2020," DW news, 2020.
- [3] A. C. Bhowmick, T. Chakrabarty, S. Akter, A. S. M. Saifullah, M. S. Sheikh, and A. C. Bhowmick, "Use of fertiliser and pesticide in Agrarian area of Tangail District, Bangladesh Medical waste management View project Urban planning View project Use of Fertilizer and Pesticide for Crop Production in Agrarian Area of Tangail District," *Environ. Ecol. Res.*, vol. 2, no. 6, (2014): pp. 253–261.
- [4] W. C. Qin, X. Y. Xue, L. F. Cui, Q. Q. Zhou, Z. F. Xu, and F. L. Chang, "Optimisation and test for spraying parameters of cotton defoliant sprayer," *Int. J. Agric. Biol. Eng.*, vol. 9, no. 4, (2016): pp. 63–72.

- [5] H. Zhang, L. Qi, Y. Wu, E. M. Musiu, Z. Cheng, and P. Wang, "Numerical simulation of airflow field from a six-rotor plant protection drone using lattice Boltzmann method," *Biosyst. Eng.*, vol. 197, (2020): pp. 336–351.
- [6] P. P. Hector Guillermo, A. M. Victor Daniel, and G. G. Elvis Eduardo "CFD Analysis of two and four blades for multirotor Unmanned Aerial Vehicle," 2018 IEEE 2nd Colomb. Conf. Robot. Autom. CCRA 2018, no. January 2019, (2018) pp. 1–6.
- [7] S. C. Zhang, X. Y. Xue, Z. Sun, L. X. Zhou, and Y. K. Jin, "Downwash distribution of single-rotor unmanned agricultural helicopter on hovering state," *Int. J. Agric. Biol. Eng.*, vol. 10, no. 5, (2017): pp. 14–24.
- [8] Q. Guo et al., "CFD simulation and experimental verification of the spatial and temporal distributions of the downwash airflow of a quad-rotor agricultural UAV in hover," Comput. Electron. Agric., vol. 172, no. December 2019, p. 105343.(2020)
- [9] S. Wen et al., "Numerical analysis and validation of spray distributions disturbed by quad-rotor drone wake at different flight speeds," Comput. Electron. Agric., vol. 166, no. February, p. 105036. (2019)

- [10] Z. Songchao, X. Xinyu, and Q. Weicai, "Simulation and experimental verification of aerial spraying drift on N-3 unmanned spraying helicopter" (2015)
- [11] Y. Zheng *et al.*, "The computational fluid dynamic modeling of downwash flow field for a six-rotor UAV," *Front. Agric. Sci. Eng.*, vol. 5, no. 2, (2018): pp. 159–167, doi: 10.15302/J-FASE-2018216.
- [12] X. Y. Xue, K. Tu, W. C. Qin, Y. Bin Lan, and H. H. Zhang, "Drift and deposition of ultra-low altitude and low volume application in paddy field," *Int. J. Agric. Biol. Eng.*, vol. 7, no. 4, (2014): pp. 23–28.
- [13] F. Yang, X. Xue, C. Cai, Z. Sun, and Q. Zhou, "Numerical simulation and analysis on spray drift movement of multirotor plant protection unmanned aerial vehicle," *Energies*, vol. 11, no. 9 (2018)
- [14] S. P. Yeong and S. S. Dol, (2016) "Aerodynamic optimisation of micro aerial vehicle," *J. Appl. Fluid Mech.*, vol. 9, no. 5, (2016): pp. 2111–2121.
- [15] H. A. Kutty and P. Rajendran, "3D CFD simulation and experimental validation of small APC slow flyer propeller blade," *Aerospace*, vol. 4, no. 1 (2017)